Inclusion of Mesoscale Updrafts and Downdrafts in Computations of Vertical Fluxes by Ensembles of Tropical Clouds

ROBERT A. HOUZE, JR., AND CHEE-PONG CHENG

Department of Atmospheric Sciences, University of Washington, Seattle, 98195

(Manuscript received 17 July 1980, in final form 14 April 1981)

ABSTRACT

Ensembles of convective clouds, especially in the tropics, often have widespread precipitating anvils associated with their deeper convective clouds. Mesoscale downdrafts occur below the middle-level bases of the anvils, and mesoscale updrafts may occur within the anvils themselves. Often, the special characteristics of these mesoscale anvil vertical motions are not taken into account in diagnosing or parameterizing the large-scale effects of cloud ensembles. This paper describes calculations of the differences in diagnosed ensemble mass and heat fluxes obtained when mesoscale motions are accounted for in comparison to when they are not. One dimensional models are used to represent both the convective-scale updrafts and downdrafts and the mesoscale anvil updrafts and downdrafts occurring within the cloud ensemble. All ensembles are constrained to account for the observed convective and anvil precipitation in Phase III of the Global Atmospheric Research Program's Atlantic Tropical Experiment (GATE). The inclusion of reasonable amounts of either mesoscale updraft or mesoscale downdraft motion or some combination of the two leads to the diagnosis of 15–20% less ensemble mass transport at low levels and 20–30% more mass flux aloft. Diagnosed heat transports in the mid to low troposphere are increased substantially by the inclusion of mesoscale downdrafts and decreased by the inclusion of mesoscale updrafts. These opposing effects on the heat flux cancel if moderate amounts of both mesoscale updraft and downdraft motions are included, and the resulting heat flux in this case differs little from one diagnosed without accounting for the mesoscale motions.

1. Introduction

This paper forms a series with four preceding papers dealing with mass and heat fluxes by ensembles of tropical clouds in GATE (Cheng and Houze, 1979; Houze *et al.*, 1980; Cheng and Houze, 1980; Leary and Houze, 1980—hereafter referred to as CH1, H, CH2 and LH, respectively). In these papers, an ensemble of tropical clouds is envisaged to consist partly of convective cells containing cumulus-scale updrafts and downdrafts and partly of mesoscale precipitating anvil clouds (Fig. 1). Here, we use the term anvil as defined by Brown (1979). It is an extensive sheet of stratiform mid-to-upper tropospheric cloud that develops when several deep tropical convective cells become organized on the mesoscale. The anvil cloud spreads out from the cells and covers the mesoscale system. The broad patches of high cloud formed by the tops of these anvils dominate satellite pictures of equatorial regions, and, in studies of satellite imagery, tropical mesoscale systems covered by anvils have been termed "cloud clusters" (Frank, 1970; Martin and Suomi, 1972). As indicated in Fig. 1, mesoscale subsidence is observed below the bases of the anvil clouds (Zipser, 1969, 1977; Betts *et al.*, 1976; Houze, 1977; Leary and Houze, 1979), and mesoscale ascent appears to occur directly above the mesoscale downdraft, i.e., in the anvil itself (Brown, 1979). In this paper, we are concerned with the possible importance of the mesoscale anvil updrafts and downdrafts in contributing to the mass and heat fluxes by an ensemble of tropical clouds.

The ensemble of clouds considered here is the one described by the GATE Phase III (mid-August to mid-September) precipitation spectrum shown in Fig. 2. This spectrum was derived from GATE radar data in CH1. It shows the percentages of the total Phase III precipitation that were seen on radar to be convective and stratiform (or mesoscale). The convective rain was intense and highly transient. It was subdivided into categories of observed maximum cell height. In contrast to the cells, the areas of mesoscale anvil rain were slowly varying, not extremely intense, horizontally homogeneous and covered regions up to 200 km in horizontal dimension. Since the anvil rain was a considerable portion of the total precipitation, and since mesoscale updrafts and downdrafts are found in the regions where such anvil rain occurs, the spectrum suggests that mesoscale drafts contributed significantly to the vertical eddy fluxes of mass and heat accomplished by GATE clouds.

Johnson (1980) found that mesoscale downdraft

0022-4928/81/081751-20$09.00

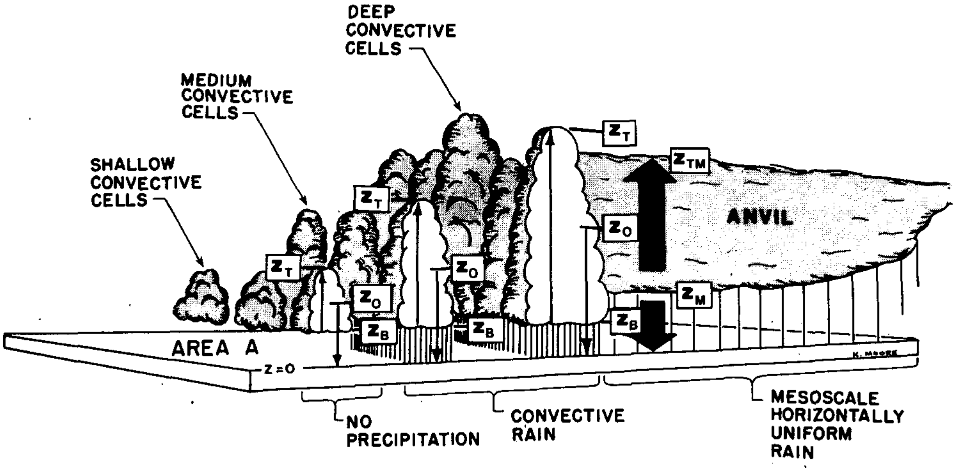

FIG. 1. Schematic of a typical population of clouds over a tropical ocean. Thin arrows represent convective-scale updrafts and downdrafts; wide arrows represent mesoscale updrafts and downdrafts. Other symbols are defined in the text and Appendix. From Houze *et al.* (1980).

motions could contribute significantly to the GATE fluxes. However, he did not calculate the possible effects of mesoscale updrafts, or combinations of mesoscale updrafts and downdrafts. In LH, the effects of the mesoscale updraft, and downdraft of a single idealized GATE mesoscale convective system were considered, and it was found that both the updraft and downdraft could substantially affect the system's vertical profiles of mass and heat transports. In this paper, we determine the extent to which the mesoscale updrafts and downdrafts contained in the various mesoscale systems that produced the anvil rain in the GATE Phase III precipitation spectrum could have acted in concert to affect the mass and heat fluxes accomplished by the entire ensemble of GATE Phase III clouds.

To accomplish this objective, we must relate the fluxes to the observed precipitation spectrum mathematically. In H, the mathematical relationships between vertical fluxes by an ensemble of tropical clouds and the precipitation spectrum were investigated and found by recognizing the relationship of the precipitation spectrum to the water budget of the cloud ensemble. We begin by reviewing that relationship.

2. Relationship of the precipitation spectrum to the water budget of an ensemble of clouds

In the notation of H (used wherever possible throughout this paper), we express the precipitation spectrum mathematically as follows:

- R_m is the total (mesoscale) rain from all the anvil clouds in the ensemble
- $R_c(\lambda)d\lambda$ is the total rain from all the convective cells in one category of cell height.

The quantity λ is the entrainment rate, which is related inversely to cell height $z_T(\lambda)$. $R_c(\lambda)d\lambda$ is thus the total rain from cells with entrainment rates in the range λ to $\lambda + d\lambda$, or from cells in the size range $z_T(\lambda)$ to $z_T(\lambda + d\lambda)$. This size range corresponds to a cell-height category such as the ones represented in discrete form by the bars in the convective portion of the histogram in Fig. 2.

Mesoscale updraft and downdraft motions are associated with R_m; convective updraft and downdraft motions are associated with $R_c(\lambda)d\lambda$.

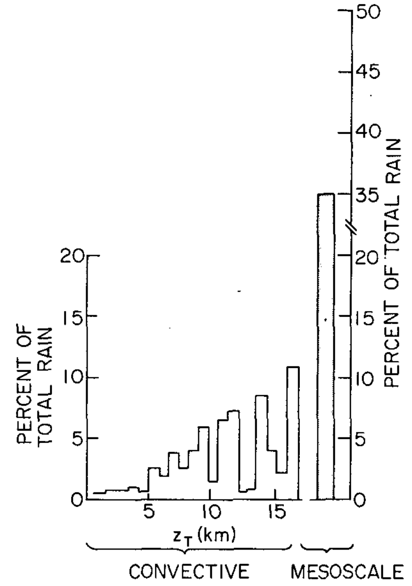

FIG. 2. Precipitation spectrum for Phase III of GATE derived from radar data. Graph shows the percentage of total GATE Phase III rainfall associated with convective cells of various heights (z_T) and with mesoscale anvil clouds. From Cheng and Houze (1979).

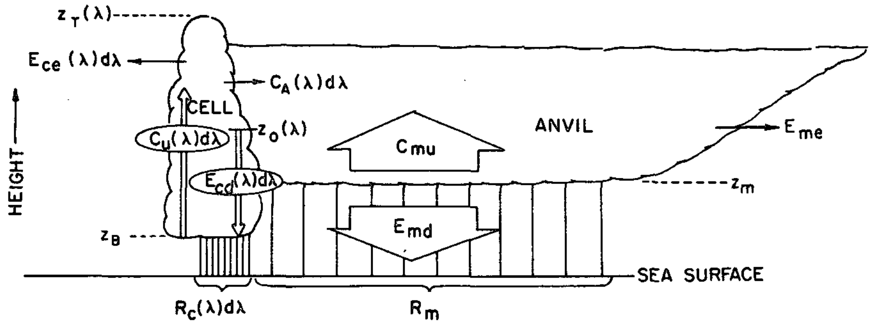

FIG. 3. Schematic showing the water budget parameters for one category of convective cell interacting with the bulk anvil cloud. The narrow upward arrow represents the convective updraft associated with condensation in the cell $C_u(\lambda)d\lambda$. The narrow downward arrow represents the convective downdraft associated with evaporation in the cell $E_{cd}(\lambda)d\lambda$. The wide upward arrow represents the mesoscale updraft associated with the condensation in the anvil C_{mu}. The wide downward arrow represents the mesoscale downdraft associated with the evaporation under the anvil E_{md}. Horizontal arrows represent condensate from the cell $[E_{ce}(\lambda)d\lambda]$ and the anvil (E_{me}) that evaporates in the large-scale environment and condensate from the cell that is incorporated into the anvil $[C_A(\lambda)d\lambda]$. $R_c(\lambda)d\lambda$ and R_m are the rainfall from the cell and the anvil, respectively. Other symbols are defined in the text and Appendix. From Houze *et al.* (1980).

If we let 1) all anvil clouds in the ensemble be similar to a model anvil cloud; and 2) all cells in a size category be similar to a model cell of height $z_T(\lambda)$; then the water budget of one size category of cell can be considered in terms of a bulk convective cloud of height $z_T(\lambda)$, which produces an amount of convective rain $R_c(\lambda)d\lambda$, interacting with a bulk anvil cloud, which produces an amount of anvil rain R_m (see Fig. 3).

In the bulk convective cloud, the mass of water condensed in the cumulus-scale updraft is represented by $C_u(\lambda)d\lambda$. The water budget of the bulk convective cloud may be expressed as

$$C_u(\lambda)d = [R_c(\lambda) + E_{cd}(\lambda) + E_{ce}(\lambda) + C_A(\lambda)]d\lambda, \quad (1)$$

where $E_{cd}(\lambda)d\lambda$ and $E_{ce}(\lambda)d\lambda$ are the portions of the condensate $C_u(\lambda)d\lambda$ that are reevaporated in cumulus-scale downdrafts and in the large-scale environment, respectively, and $C_A(\lambda)d\lambda$ is the portion of $C_u(\lambda)d\lambda$ that is incorporated into the mesoscale anvil cloud, either by being detrained from the upper portions of active cells, or by being left aloft by dying cells that blend into the anvil cloud when new cells form adjacent to the anvil (Houze, 1977; Leary and Houze, 1979). Expressing the terms on the right-hand side of (1) as fractions of the condensate $C_u(\lambda)d\lambda$, we obtain

$$R_c(\lambda)d\lambda = \nu_c(\lambda)C_u(\lambda)d\lambda, \quad (2)$$

$$E_{cd}(\lambda)d\lambda = \alpha(\lambda)C_u(\lambda)d\lambda, \quad (3)$$

$$E_{ce}(\lambda)d\lambda = \beta(\lambda)C_u(\lambda)d\lambda, \quad (4)$$

$$C_A(\lambda)d\lambda = \eta(\lambda)C_u(\lambda)d\lambda, \quad (5)$$

where $\nu_c(\lambda)$, $\alpha(\lambda)$, $\beta(\lambda)$ and $\eta(\lambda)$ are each either zero or a positive fraction. To be consistent with (1), they must satisfy the constraint that

$$\nu_c(\lambda) + \alpha(\lambda) + \beta(\lambda) + \eta(\lambda) = 1. \quad (6)$$

In the bulk anvil cloud, the mass of water condensed in the anvil's mesoscale updraft is represented by C_{mu}. The anvil cloud consists partly of this condensate and partly of water introduced into the anvil through the effects represented by $C_A(\lambda)d\lambda$ in Eq. (1) and Fig. 3. Thus, the water budget of the anvil may be expressed by

$$C_{mu} + C_A^* = R_m + E_{md} + E_{me}, \quad (7)$$

where

$$C_A^* = \int_0^\infty C_A(\lambda)d\lambda, \quad (8)$$

E_{md} is the portion of $(C_{mu} + C_A^*)$ that is reevaporated in the mesoscale downdraft below the base of the anvil cloud, and E_{me} is the portion of $(C_{mu} + C_A^*)$ that is detrained or left aloft by the anvil cloud to be reevaporated in the large-scale environment. Expressing the terms on the right-hand side of (7) as fractions of $(C_{mu} + C_A^*)$, we obtain

$$R_m = \nu_m(C_{mu} + C_A^*), \quad (9)$$

$$E_{md} = a(C_{mu} + C_A^*), \quad (10)$$

$$E_{me} = b(C_{mu} + C_A^*), \quad (11)$$

where ν_m, a and b are zero or positive fractions, which, to be consistent with (7), must satisfy the constraint

$$\nu_m + a + b = 1. \quad (12)$$

The parameters $\nu_c(\lambda)$ and ν_m introduced in (2) and (9), respectively, are precipitation efficiencies: $\nu_c(\lambda)$ is the efficiency with which the condensate produced in the convective updraft of the bulk cell is converted to precipitation; and ν_m is the efficiency with which condensate in the anvil cloud is converted to mesoscale anvil precipitation (R_m). The efficiencies ν_c and ν_m, as well as the other water budget parameters, α, β, η, a and b, in (2)–(12) must be known or assumed in order to relate the precipitation amounts R_m and $R_c(\lambda)d\lambda$ to condensation in updrafts [$C_u(\lambda)d\lambda$ and C_{mu}] and evaporation in downdrafts [$E_{cd}(\lambda)d\lambda$ and E_{md}]. Further assumptions (dealing with mass transport profiles, entrainment rates and the thermodynamical properties of the air in the updrafts and downdrafts) allow the condensation to be related, in turn, to the mass and heat fluxes of updrafts and the evaporation to be related to the mass and heat fluxes of downdrafts.

This paper is concerned with the first type of assumption, that is, of values for the water budget parameters relating condensation and evaporation to precipitation. In many diagnostic studies of tropical convection, the values of these water budget parameters have been chosen, either explicitly or tacitly, so that

$$C_{mu} = 0 \tag{13}$$

and

$$E_{md} = 0. \tag{14}$$

Under such assumptions, no mesoscale anvil updrafts or downdrafts can occur in the ensemble of model clouds. Consequently, mass and heat fluxes are diagnosed as if mesoscale anvil circulations do not exist. In this paper, we consider all the possible combinations of water budget parameters that can be argued to be physically reasonable for Phase III of GATE. These combinations give all possible values of C_{mu} and E_{md}, which, in turn, can be related to mesoscale updraft and downdraft motions and hence to all the possible contributions of mesoscale anvil circulations to cloud mass and heat fluxes during Phase III of GATE.

3. Relationship of mass and heat flux to the cloud ensemble water budget

To evaluate the impact of mesoscale anvil vertical motions on the GATE Phase III mass and heat fluxes, we relate these fluxes to the cloud ensemble water budget parameters defined in the foregoing section. Mathematical formulas for this purpose, developed in H, are briefly reviewed in this section.

a. Subdivision of fluxes into convective and mesoscale components

We consider the average vertical fluxes over a large-scale area A and time τ by an ensemble of clouds located within A. In this study, A is the area covered by the GATE B-scale ship array (0.6×10^5 km^2) and τ is the time period of Phase III of GATE (21 days). It is convenient to subdivide the fluxes into convective and mesoscale components by expressing them as

$$M(p) = M_c(p) + M_m(p) \tag{15}$$

and

$$\mathcal{H}(p) = \mathcal{H}_c(p) + \mathcal{H}_m(p), \tag{16}$$

where $M(p)$ and $\mathcal{H}(p)$, respectively, are the vertical fluxes of mass and heat through pressure-level p. The subscripts c and m refer to the contributions of the vertical motions associated with convective cells and mesoscale anvil clouds, respectively.

We may express the convective-scale mass flux M_c as the integrated contributions of cells of different sizes by writing

$$M_c(p) = \frac{1}{A\tau}\int_0^{\lambda_T(p)} [\mathcal{M}_u(\lambda, p) + \mathcal{M}_d(\lambda, p)]d\lambda, \tag{17}$$

where $\mathcal{M}_u(\lambda, p)d\lambda$ and $\mathcal{M}_d(\lambda, p)d\lambda$ are the masses of air transported vertically through level p in the convective-scale updrafts and downdrafts, respectively, of cells with entrainment rates λ to $\lambda + d\lambda$, and $\lambda_T(p)$ is the entrainment rate for cells with tops at level p.

The mass flux by mesoscale anvil vertical motions may be written as

$$M_m(p) = \frac{\mu_m(p)}{A\tau}, \tag{18}$$

where $\mu_m(p)$ is the mass transported vertically through level p in mesoscale drafts. The heat flux terms $\mathcal{H}_c(p)$ and $\mathcal{H}_m(p)$ may be written in terms of updraft and downdraft properties as follows:

$$\mathcal{H}_c(p) = \frac{1}{A\tau}\int_0^{\lambda_T(p)} \{\mathcal{M}_u(\lambda, p)[h_u(\lambda, p) - \tilde{h}_e(p)] + \mathcal{M}_d(\lambda, p)[h_d(\lambda, p) - \tilde{h}_e(p)]\}d\lambda, \tag{19}$$

$$\mathcal{H}_m(p) = \frac{\mu_m(p)}{A\tau}[h_m(p) - \tilde{h}_e(p)], \tag{20}$$

where h_u, h_d, h_m and $\tilde{h}_e$ are the moist static energies in convective updrafts, convective downdrafts, mesoscale drafts and the large-scale environment, respectively.

Eq. (16) is equivalent to Eq. (59) of H. The probably small term $\widetilde{\sigma_m\overline{\omega(p)}}$ defined in H and included in (H59)[1] is ignored in (20) in comparison to $\mu_m/A\tau$.

b. Formulation of convective fluxes

In H, $\mathcal{M}_u(\lambda, p)$ is equated to the product of the cell base mass flux spectral parameter $\mathcal{M}_B(\lambda)$ and

---

[1] Equations in H are hereafter indicated by prefix H.

vertical profile of convective updraft mass flux $f_u[\lambda, z(p)]$, where z is height, as follows:

$$\mathcal{M}_u(\lambda, p) = \mathcal{M}_B(\lambda) f_u[\lambda, z(p)] \tag{21}$$

[see Eq. (H3)]. In (H36), $\mathcal{M}_B(\lambda)$ is related to the convective precipitation $R_c(\lambda)d\lambda$ and the convective precipitation efficiency $\nu_c(\lambda)$ through

$$\mathcal{M}_B(\lambda)d\lambda = \frac{R_c(\lambda)d\lambda}{\nu_c(\lambda)I_1(\lambda)}, \tag{22}$$

where $I_1(\lambda)$, defined by (H37), depends on the water vapor mixing ratio in the convective updrafts and in the environment. In H, $\mathcal{M}_d(\lambda, p)$ is related to the cell base mass flux parameter $\mathcal{M}_B(\lambda)$ and vertical profile of convective downdraft mass flux $f_d[\lambda, z(p)]$ by the relation

$$\mathcal{M}_d(\lambda, p) = \epsilon(\lambda)\mathcal{M}_B(\lambda) f_d[\lambda, z(p)], \tag{23}$$

where $\epsilon(\lambda)$ is an expression of the reevaporation of convective condensate in convective-scale downdrafts and is given by

$$\epsilon(\lambda) = \frac{\alpha(\lambda)I_1(\lambda)}{I_2(\lambda)}, \tag{24}$$

where $I_2(\lambda)$, defined by (H39), depends on the water vapor mixing ratios in the convective downdrafts and in the environment. [Eq. (23) is obtained by combining (H17) and (H41). Eq. (24) is the same as (H42).]

Expressions for $\mathcal{M}_u(\lambda, p)$ and $\mathcal{M}_d(\lambda, p)$ obtained by combining (22) and (24) with (21) and (23) are

$$\mathcal{M}_u(\lambda, p)d\lambda = \frac{R_c(\lambda) f_u[\lambda, z(p)]d\lambda}{\nu_c(\lambda)I_1(\lambda)}, \tag{25}$$

$$\mathcal{M}_d(\lambda, p)d\lambda = \frac{\alpha(\lambda)R_c(\lambda) f_d[\lambda, z(p)]d\lambda}{\nu_c(\lambda)I_2(\lambda)}. \tag{26}$$

Thus, as shown by Austin and Houze (1973), the mass flux in convective updrafts ($\mathcal{M}_u d\lambda$) in a given cloud-size category (λ to $\lambda + d\lambda$) is given by the convective precipitation ($R_c d\lambda$), the convective precipitation efficiency (ν_c) and large-scale environmental thermodynamic conditions (contained in I_1). As shown by Houze and Leary (1976), the mass flux in convective downdrafts ($\mathcal{M}_d d\lambda$) is obtained by an analogous relationship, with the additional involvement of the water budget parameter α, which expresses the fraction of convective condensate reevaporated in convective-scale downdrafts.

Expressions for the mass and heat fluxes by the convective-scale updrafts and downdrafts can now be obtained by substituting (25) and (26) into (17) and (19). The resulting equations are

$$M_c(p) = \frac{1}{A\tau}\int_0^{\lambda_T(p)} \left\{ \frac{R_c(\lambda)}{\nu_c(\lambda)} \frac{f_u[\lambda, z(p)]}{I_1(\lambda)} + \frac{\alpha(\lambda)R_c(\lambda)}{\nu_c(\lambda)} \frac{f_d[\lambda, z(p)]}{I_2(\lambda)} \right\} d\lambda, \tag{27}$$

$$\mathcal{H}_c(p) = \frac{1}{A\tau}\int_0^{\lambda_T(p)} \left\{ \frac{R_c(\lambda)}{\nu_c(\lambda)} \frac{f_u[\lambda, z(p)]}{I_1(\lambda)} \times [h_u(\lambda, p) - \tilde{h}_e(p)] + \frac{\alpha(\lambda)R_c(\lambda)}{\nu_c(\lambda)} \times \frac{f_d[\lambda, z(p)]}{I_2(\lambda)} [h_d(\lambda, p) - \tilde{h}_e(p)] \right\} d\lambda. \tag{28}$$

These equations express the mass and heat fluxes by convective-scale vertical motions in terms of the amounts of condensation in convective updrafts $[R_c(\lambda)d\lambda/\nu_c(\lambda)]$ and evaporation in convective downdrafts $[\alpha(\lambda)R_c(\lambda)d\lambda/\nu_c(\lambda)]$.

c. Formulation of mesoscale updraft fluxes

Above the tops of the anvil downdrafts (level z_M in Figs. 1 and 3), the mass and heat fluxes by anvil cloud vertical air motions are determined only by mesoscale updrafts, and (18) and (20) may be written as

$$M_m(p) = \frac{\mu_{mu}(p)}{A\tau}, \quad p < p(z_M), \tag{29}$$

$$\mathcal{H}_m(p) = \frac{\mu_{mu}(p)}{A\tau}[h_{mu}(p) - \tilde{h}_e(p)], \quad p < p(z_M), \tag{30}$$

where $\mu_{mu}(p)$ is the mass transported vertically through level p in the mesoscale updrafts and h_{mu} is the moist static energy in the mesoscale updrafts. In H, it is shown that $\mu_{mu}(p)$ may be expressed by a relationship analogous to (26), specifically,

$$\mu_{mu}(p) = \frac{C_{mu} f_{mu}[z(p)]}{I_3}, \quad p < p(z_M). \tag{31}$$

This relation [obtained by combining (H24) and (H50)] expresses the mass transported vertically in the mesoscale updraft μ_{mu} [which is analogous to $\mathcal{M}_u d\lambda$ in (25)] in terms of the total condensation C_{mu} produced by the mesoscale updraft [analogous to $R_c d\lambda/\nu_c$ in (25)], the vertical profile of the mesoscale updraft mass flux f_{mu} [analogous to f_u in (25)] and the quantity I_3 [analogous to I_1 in (25)], which is defined by (H51) and determined from the mixing ratio in the mesoscale updraft (see Section 4). Substitution of (31) into (29) and (30) leads to

$$M_m(p) = \frac{C_{mu} f_{mu}[z(p)]}{A\tau I_3}, \quad p < p(z_M), \tag{32}$$

$$\mathscr{H}_m(p) = \frac{C_{mu} f_{mu}[z(p)]}{A\tau I_3}\,[h_{mu}(p) - \tilde{h}_e(p)],$$
$$p < p(z_M), \tag{33}$$

which express the mass and heat fluxes by anvil updrafts in terms of the amount of condensation C_{mu} that occurs in them.

d. Formulation of mesoscale downdraft fluxes

Below the tops of the anvil downdrafts (level z_M in Figs. 1 and 3), the mass and heat fluxes by anvil cloud vertical air motions are determined only by mesoscale downdrafts, and (18) and (20) are given by

$$M_m(p) = \frac{\mu_{md}(p)}{A\tau}, \quad p \geqslant p(z_M), \tag{34}$$

$$\mathscr{H}_m(p) = \frac{\mu_{md}(p)}{A\tau}\,[h_{md}(p) - \tilde{h}_e(p)], \quad p \geqslant p(z_M), \tag{35}$$

where $\mu_{md}(p)$ (a negative quantity) is the mass transported vertically through level p in the mesoscale downdrafts and h_{md} is the moist static energy in the mesoscale downdrafts. In H, it is shown that $\mu_{md}(p)$ may be expressed by a relation analogous to (26), specifically,

$$\mu_{md}(p) = \frac{E_{md} f_{md}[z(p)]}{I_4}, \quad p \geqslant p(z_M), \tag{36}$$

where $f_{md}[z(p)]$ is a negative quantity. This relation [obtained by combining (H25), (H47) and (H56)] expresses the mass transported vertically in mesoscale downdrafts μ_{md} [analogous to $\mathscr{M}_d d\lambda$ in (26)] in terms of the total evaporation E_{md} in the mesoscale downdraft [analogous to $\alpha R_c d\lambda/\nu_c$ in (26)], the vertical profile of the mesoscale downdraft mass flux f_{md} [analogous to f_d in (26)] and the quantity I_4 [analogous to I_2 in (26)], which is defined by (H55) and determined from the mixing ratio in the mesoscale downdraft (see Section 4). Substitution of (36) into (34) and (35) leads to

$$M_m(p) = \frac{E_{md} f_{md}[z(p)]}{A\tau I_4}, \quad p \geqslant p(z_M), \tag{37}$$

$$\mathscr{H}_m(p) = \frac{E_{md} f_{md}[z(p)]}{A\tau I_4}\,[h_{md}(p) - \tilde{h}_e(p)],$$
$$p \geqslant p(z_M) \tag{38}$$

which express the mass and heat fluxes by anvil downdrafts in terms of the amount of evaporation E_{md} that occurs in them.

e. Mesoscale condensation and evaporation as indicators of the contributions of anvil air motions to cloud ensemble fluxes

From (32), (33), (37) and (38), it is evident that the mass and heat transports by anvil updrafts are directly proportional to the amount of condensate C_{mu} produced by the lifting in the mesoscale updrafts and that the transports by anvil downdrafts are directly proportional to the amount of evaporation E_{md} produced by sinking in the mesoscale downdrafts. In this study, the magnitude of anvil updraft and downdraft contributions to the cloud ensemble heat flux $\mathscr{H}(p)$ are examined through analysis of the terms C_{mu} and E_{md} (Section 7). We have already noted in Eqs. (13) and (14) that assuming mesoscale motions do not contribute to $\mathscr{H}(p)$ at all is equivalent to assuming $C_{mu} = E_{md} = 0$. In this study, we examine cases in which mesoscale motions do contribute to $\mathscr{H}(p)$ by considering the conditions under which C_{mu} and E_{md} are nonzero.

From (9) and Fig. 3, it is evident that

$$C_{mu} = \frac{R_m}{\nu_m} - C_A^*, \tag{39}$$

where the first term on the right is equal to the total condensate making up the anvil cloud, and C_A^* is the portion of this total condensate that was obtained by incorporation of hydrometeors into the anvil from neighboring cells, by being detrained from active cells or left aloft by dying cells. C_{mu} is the portion of the total condensate generated within the anvil itself by mesoscale lifting. With substitution from (2), (5) and (8), (39) may be written as

$$C_{mu} = \frac{R_m}{\nu_m} - \int_0^\infty \eta(\lambda)\left[\frac{R_c(\lambda)}{\nu_c}\right]d\lambda. \tag{40}$$

From this expression, C_{mu} is seen to be related (i) to the mesoscale anvil precipitation R_m and the efficiency ν_m with which it is converted microphysically from anvil cloud condensate to anvil precipitation; (ii) to the convective precipitation $R_c(\lambda)d\lambda$ and the efficiency ν_c with which it is converted from convective cell condensate to precipitation; and (iii) to the effectiveness [represented by $\eta(\lambda)$] with which the convective condensate is incorporated into the anvil from neighboring cells.

Note that if $\eta(\lambda)$ is zero for all λ, the second term in (40) vanishes and all the anvil precipitation must be explained by mesoscale updraft condensate. By contrast if $\eta(\lambda)$ is large, the second term in (40) can cancel the first term. In this case all the anvil precipitation is explained by transfer of condensate into the anvil from cells and no mesoscale updraft is required ($C_{mu} = 0$).

By combining (9) and (10), we obtain

$$E_{md} = \frac{aR_m}{\nu_m}. \tag{41}$$

From this expression, it can be seen that, like C_{mu}, E_{md} is related to R_m and ν_m. It is also related to the water budget parameter a, which expresses the fraction of anvil condensate evaporated in the mesoscale downdraft.

In most previous diagnostic studies of deep convection, it has been assumed either explicitly or implicitly that the water budget parameters ν_m, ν_c and η have values such that the two terms on the right in (40) cancel and $C_{mu} = 0$. That is, no mesoscale updraft motion is allowed. Any anvil precipitation that occurs is, consequently, assumed to be explained by condensation in convective cells associated with the anvils. In this paper, we consider all the physically plausible combinations of water budget parameters, including cases for which $C_{mu} \neq 0$ as well as those for which $C_{mu} = 0$.

It also has been typically assumed, either explicitly or implicitly, that the parameter a has the value zero in (41). In this paper, we consider all the physically plausible cases for which a, and, hence, E_{md}, are nonzero.

From (40) and (41), it is evident that the choices of the water budget parameters ν_c, ν_m, η and a determine the values of C_{mu} and E_{md}, which, in turn, according to (32), (33), (37) and (38), determine the magnitudes of the mesoscale anvil contributions to the cloud ensemble mass and heat fluxes. Therefore, by identifying the physically reasonable values of the water budget parameters, we can determine the sensitivity of the ensemble mass and heat fluxes to the mesoscale anvil circulations.

4. Procedure for computing mass and heat fluxes

In computing the mass and heat fluxes for various combinations of water budget parameters, we work with the "radar approach," using the precipitation spectrum as input. However, results regarding the sensitivity of the calculation to assumed values of water budget parameters should be equally applicable to the "synoptic approach," in which large-scale heat and moisture budgets are used as input. In H, it is shown that both approaches are based on the same basic equations, and, therefore, can be expected to respond similarly to changes in assumed values of parameters that appear in the equations.

The procedure followed in this study is to calculate $M(p)$ from (15) and $\mathcal{H}(p)$ from (16), with $M_c(p)$ given by (27), $\mathcal{H}_c(p)$ given by (28), $M_m(p)$ and $\mathcal{H}_m(p)$ given by (32) and (33) for p above the top of the anvil downdrafts $[p < p(z_m)]$ and by (37) and (38) for p below the top of the anvil downdrafts $[p \geqslant p(z_m)]$. The values of C_{mu} and E_{md}, which appear in (32), (33), (37) and (38) can be computed from (40) and (41). [Actually, C_{mu} and E_{md} are computed from simplified versions of (40) and (41), given by (64) and (65) in Sec. 7.]

To compute $M_c(p)$, $\mathcal{H}_c(p)$, $M_m(p)$ and $\mathcal{H}_m(p)$ from (27), (28), (32), (33), (37), (38), (40) [or (64)] and (41) [or (65)], the following quantities must be given or assumed: $R_c(\lambda)d\lambda$, R_m, h_e, h_u, h_d, h_{mu}, h_{md}, I_1, I_2, I_3, I_4, f_u, f_d, f_{mu}, f_{md}, $\lambda_T(p)$, ν_c, ν_m, α, a and η. Values of the precipitation amounts $R_c(\lambda)d\lambda$ and R_m are determined by applying the observed precipitation spectrum in Fig. 2, which is expressed in percentages, to the GATE Phase III rainfall observed over the B-scale ship array (25.6 cm). The observed mean thermodynamic conditions in the large-scale environment during Phase III of GATE (Thompson *et al.*, 1979) are used to obtain $\bar{h}_e$.[2] The quantities h_u, h_d, h_{mu}, h_{md}, I_1, I_2, I_3, I_4 and $\lambda_T(p)$ are computed using the large-scale environment conditions as input to one-dimensional steady-state plume models for the convective-scale updrafts and downdrafts and simple bulk models of the mesoscale anvil updraft and downdraft (see Appendix and H for details). The profile shapes assumed for f_u, f_d, f_{mu} and f_{md} and the entrainment rate function $\lambda_T(p)$ are those recommended in CH2 and used in LH (See Appendix). The water budget parameters representing precipitation efficiencies (ν_c and ν_m), downdraft evaporation (α and a) and incorporation of convective condensate into anvil clouds (η) have to be assumed. The sensitivity of the mass and heat flux calculations to the values assumed for these water budget parameters is the subject of this paper. Our procedure for identifying the most reasonable combinations of water budget parameters for use in computing the mass and heat fluxes is described in Sections 5–7 below, and the profiles of mass and heat flux obtained for extreme and realistic combinations of these water budget parameters are described in Section 8.

5. Criteria for identifying physically reasonable values of the water budget parameters

a. Possible combinations

Little is known about the water budget parameters, ν_c, ν_m, α, a and η, which have to be assumed to calculate the cloud ensemble mass and heat fluxes, except that each may take on values from 0 to 1. Many combinations are possible. Any combination, however, must satisfy the constraints (6) and (12), which involve the additional parameters β and b, which represent evaporation of cloud condensate in the large-scale environment. The number of possible combinations of ν_c, ν_m, α, a, η, β and b can be reduced by eliminating from consideration or de-emphasizing any combinations that lead to physically unreasonable conclusions. In Sections 5b–5f below, we discuss five criteria, or constraints, that are used to eliminate unreasonable combinations of values so that we may focus attention on the most realistic combinations.

b. Constraint on mesoscale updraft condensation

From (5), (7) and (8)–(11), it is evident that there exist combinations of the parameters η, ν_m, a and b

---

[2] A better approach might be to determine the precipitation spectrum on a daily basis and use daily observations of environment conditions. However, the use of Phase III totals and means should be sufficient to obtain the conclusions sought in this study.

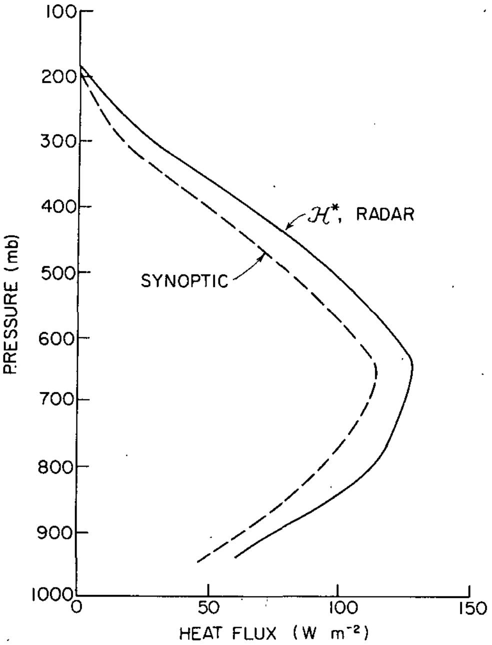

FIG. 4. Vertical eddy fluxes of sensible plus latent heat by vertical motions associated with clouds in the GATE B-scale ship array during Phase III of GATE. "Synoptic" curve is deduced from heat and moisture budgets based on ship sounding data (see text for details). "Radar" curve, denoted $\mathcal{H}^*$, is computed from radar data under the assumption that no mesoscale anvil updrafts or downdrafts affected the heat flux.

that can lead to negative values of the mesoscale updraft condensation C_{mu}. Since negative condensation is unrealistic, these combinations of parameters are eliminated from consideration by requiring that

$$C_{mu} \geqslant 0. \tag{42}$$

c. *Constraint on the heat flux at upper levels*

This constraint requires that the ensemble heat flux not deviate significantly at upper levels (above 600 mb) from the heat flux obtained when the assumed water budget parameters allow no mesoscale anvil vertical motions. This constraint is based on Fig. 4, which shows the ensemble heat flux, $\mathcal{H}(p) = \mathcal{H}^*(p)$, computed for a combination of water budget parameters which allows no mesoscale motions. The water budget parameters used in computing $\mathcal{H}^*(p)$ are prescribed (details given in Sections 6–7 below) so as to require both C_{mu} and E_{md} to be zero. This, in turn, according to (32), (33), (37) and (38), requires the mesoscale mass and heat fluxes M_m and $\mathcal{H}_m$ to be zero. In Fig. 4, $\mathcal{H}^*(p)$ is compared with the "synoptic" heat flux profile obtained in H from the large-scale GATE Phase III heat budget of Thompson *et al.* (1979). Above 600 mb, the synoptic curve is simply the residual of large-scale terms in the heat budget for the GATE B-scale array. Therefore, it contains the effects of all mesoscale and convective motions and involves no model assumptions. Below 600 mb, the effects of model clouds with tops below this height were subtracted from the synoptic curve in H to make it comparable with curves such as $\mathcal{H}^*(p)$, which are computed from the observed precipitation amounts $R_c(\lambda)d\lambda$ and R_m, according to the procedure described in Section 4, and thus contain only the effects of precipitating clouds. Since the precipitating clouds tend to be those with tops extending above the 600 mb level, it was necessary to make this correction to the synoptic curve (see H for further details). Hence, below the 600 mb level, the synoptic curve is model-dependent. Concentrating on the portion of the synoptic curve above 600 mb, we note that $\mathcal{H}^*(p)$ is generally within about 30% of the synoptic curve. Although $\mathcal{H}^*(p)$, which was based on radar precipitation data, showed larger values than the synoptic curve at all levels above 600 mb, sampling fluctuations or imperfections of either the radar or synoptic data could have led to either curve showing slightly larger values.

By changing the water budget parameters from those used to obtain the radar curve $\mathcal{H}^*(p)$ in Fig. 4, we can obtain alternate heat flux profiles and compare them with $\mathcal{H}^*(p)$. In particular, we may obtain heat flux profiles for cases where the water budget parameters allow C_{mu} and $E_{md} > 0$. Thus, differences in the profiles that arise when mesoscale motions are assumed to occur in observed anvil clouds may be seen. Examples of such profiles will be shown in Section 8.

Taking the comparison of the radar and synoptic curves in Fig. 4 as an indication of inherent uncertainty in the data, and requiring that uncertainty associated with water budget parameters be no greater than the observational uncertainty, we adopt as a criterion of acceptability that any profile $\mathcal{H}(p)$ obtained using an alternate set of water budget parameters be within 30% of $\mathcal{H}^*(p)$. Accordingly, we should require that $\mathcal{H}$ satisfy the integral constraint

$$\int_{500\text{ mb}}^{0} |\mathcal{H}(p) - \mathcal{H}^*(p)|dp \leqslant 0.3 \int_{500\text{ mb}}^{0} |\mathcal{H}^*(p)|dp. \tag{43}$$

In this constraint, only the portions of the curve above the 500 mb (rather than 600 mb) level are considered in order to avoid not only the effects of nonprecipitating clouds, whose tops are generally below 600 mb, but also to gain computational simplicity by not having to include downdraft terms in $\mathcal{H}(p)$, since all the downdrafts in the cloud ensemble originate below 500 mb (see Appendix).

The contributions of $|\mathcal{H}(p) - \mathcal{H}^*(p)|$ and $|\mathcal{H}^*(p)|$ to their respective integrals in (43) may be neglected above the 285 mb (10 km level). Therefore the constraint (43) may be replaced by

$$\int_{500\text{ mb}}^{285\text{ mb}} |\mathscr{H}(p) - \mathscr{H}^*(p)|dp \leq 0.3 \int_{500\text{ mb}}^{285\text{ mb}} |\mathscr{H}^*(p)|dp. \quad (44)$$

This constraint may be rewritten as

$$\int_{500\text{ mb}}^{285\text{ mb}} \Delta(p)|\mathscr{H}^*(p)|dp \leq 0.3 \int_{500\text{ mb}}^{285\text{ mb}} |\mathscr{H}^*(p)|dp, \quad (45)$$

where

$$\Delta(p) \equiv \frac{|\mathscr{H}(p) - \mathscr{H}^*(p)|}{|\mathscr{H}^*(p)|}. \quad (46)$$

It may be verified by inspection of computed $\mathscr{H}$ and $\mathscr{H}^*$ profiles (such as those in Figs. 8b and 9b, to be discussed in Section 8) that if

$$\Delta\,(285\text{ mb}) = \frac{|\mathscr{H}\,(285\text{ mb}) - \mathscr{H}^*\,(285\text{ mb})|}{|\mathscr{H}^*\,(285\text{ mb})|} \leq 0.3, \quad (47)$$

then $\Delta(p) \leq 0.3$ for all p between 500 and 285 mb. We verified this result for $\mathscr{H}(p)$ curves computed with various assumed shapes of the mesoscale updraft profile $f_{mu}(p)$ (using $z_{\max} = 7$ and 10 km) and different values of $h_{mu}(p)$ (using $\Delta T = 0.5$, 1.0 and 1.5°C). See Appendix for definitions of $z_{\max}$ and ΔT. Thus, (45) is satisfied whenever (47) is satisfied. However, (47) does not identify *all* the possible profiles $\mathscr{H}(p)$ that satisfy (45). We used (47) for simplicity since it involves computations at only one level. Our results, therefore, will be more conservative than if (45) had been used, since by using (47) we do not allow $\mathscr{H}(p)$ to deviate as much from $\mathscr{H}^*(p)$ as would be allowed by (45). In this way, we will tend toward understatement rather than overstatement of the possible effects of mesoscale motions on cloud ensemble fluxes.

In (43)–(47), we use the radar curve $\mathscr{H}^*(p)$ rather than the synoptic curve of H as the reference to which the heat flux profiles $\mathscr{H}(p)$, computed for various sets of water budget parameters, are tested. Use of $\mathscr{H}^*(p)$ as the reference ensures that, as long as the same precipitation spectrum is used as input, any differences in $\mathscr{H}(p)$ obtained by the procedure outlined in Section 4 and the reference profile $\mathscr{H}^*(p)$ are due solely to changes in the assumed values of the water budget parameters. The difference between a profile $\mathscr{H}(p)$ computed by the procedure outlined in Section 4 and the synoptic curve of H, on the other hand, could be attributed partly to differences between the radar and synoptic data, and this part of the difference would not be easily separable from that owing to the variation of the water budget parameters used to calculate $\mathscr{H}(p)$.

d. *Constraint on the heat flux at the top of the subcloud layer*

In addition to constraining the heat flux in the upper troposphere, we require that the heat flux profile $\mathscr{H}(p)$ computed for a given set of water budget parameters not have a value at the convective cell base level (z_B in Figs. 1 and 3) that is larger than heat fluxes observed in the subcloud layer. GATE surface and boundary-layer observations show that the heat flux at the sea surface in GATE was typically ~120 W m^{-2} (Fig. 9 of Thompson *et al.*, 1979). The total heat flux at the top of the subcloud layer should have approximately this value. The profile $\mathscr{H}(p)$ that we compute is the contribution only of precipitating clouds to the total heat flux. Small, non-precipitating cumuli also occur in great numbers in the GATE area. While it is beyond the scope of this study to quantify the exact contribution of non-precipitating clouds to the total GATE Phase III heat flux, it is reasonable to assume that they contribute substantially to the total flux at the top of the GATE subcloud layer. Accordingly, we consider a cloud base heat flux of more than 100 W m^{-2} by the ensemble of precipitating clouds alone to be unlikely, since it would disallow a significant contribution by non-precipitating clouds. Specifically, we require that the heat flux by precipitating cloud be limited at the top of the subcloud layer by the constraint,

$$\mathscr{H}(p_B) \leq 100\text{ W m}^{-2}, \quad (48)$$

where p_B is the pressure at level z_B.

e. *Constraint on the convective precipitation efficiency*

Another constraint on the possible combinations of water budget parameters used in our calculations is found by considering the precipitating efficiency of convective cells ν_c defined as the ratio of convective precipitation to condensation in convective updrafts [cf., Eq. (2)]. An empirical value of $\nu_c = 0.19$ was obtained by Braham (1952) for an average individual cell within air mass thunderstorms in Ohio and Florida. Considering Braham's study as well as radar observations of New England precipitation, Austin and Houze (1973) estimated that the precipitation efficiency of individual convective cells was ≈0.33. A precipitation efficiency of 0.56 is implied by Betts' (1973) analysis of tropical continental cumulonimbus clouds, while 53–62% is indicated by Newton's (1966) study of a midlatitude severe thunderstorm. However, the values of Betts and Newton apply to a thunderstorm as a whole, which has mesoscale dimensions, rather than to individual convective cells embedded within the storm. The efficiency of the thunderstorm as a whole must be greater than or equal to that of its individual cells (ν_c), since some of the condensate lost from cells may fall as precipitation from other parts of the thunderstorm, for example, as anvil rain. Hence, Betts' larger efficiency is consistent with the smaller efficiencies of individual cells suggested by Braham (1952) and Austin and Houze (1973).

Though the empirical information about the precipitation efficiency of individual convective cells is limited, rather small values, say,

$$0.2 \leq \nu_c \leq 0.55, \tag{49}$$

are suggested. The studies referred to were not for moist environments like that of GATE, where some of the factors contributing to inefficiency, namely, evaporation and entrainment, may have been less important than in the referenced studies. Therefore, somewhat higher efficiencies than indicated by (49) might have been possible in GATE. On the other hand, loss of condensate by detrainment or by being left aloft by a dying cell [term $C_A(\lambda)d\lambda$ in Eq. (1) and Fig. 3] is probably the major contributor to inefficiency of individual cells, and this process is not directly affected by the humidity of the large-scale environment. In this paper, we bear these unknown factors in mind but regard any values of ν_c inside the range indicated in (49) as being more likely than those outside the range.

f. Constraints on mesoscale updraft and downdraft motions

The final constraints we consider are found by examining the magnitudes of the mesoscale updraft and downdraft vertical velocities implied by our results. By computing the mesoscale mass flux $M_m(p)$ as a contribution to the average mass flux over the large-scale area A and time τ, we have avoided the question of the vertical velocities in and below the anvil clouds themselves. In (18), the expression for $M_m(p)$, we use only the total mass of air $\mu_m(p)$ transported through a level p without regard to its rate of transport, i.e., its vertical velocity. Our procedure, outlined in Section 4, determines $\mu_m(p)$ from rainfall observations (plus thermodynamic conditions in the large-scale environment, water budget parameters and other assumptions). Vertical velocity never enters the calculation of $M_m(p)$. The mass of air $\mu_m(p)$, however, may be written as

$$\mu_m(p) = \rho_m(p)w_m(p)A_m\tau_m, \tag{50}$$

where ρ_m is density, w_m is the mean vertical velocity in the horizontal area A_m covered by anvil cloud, and τ_m is the total anvil duration. Substituting (50) in (18) and rearranging terms, we obtain

$$w_m(p) = \frac{M_m(p)A\tau}{\rho_m(p)A_m\tau_m}. \tag{51}$$

This relationship determines the value of the mesoscale vertical velocity $w_m(p)$ implied by our computed value of $M_m(p)$. A_m, τ_m and ρ_m must be known.

To estimate A_m and τ_m for Phase III of GATE, we consider the sample of data from the ship *Oceanographer's* radar used in CH1 to obtain the precipitation spectrum in Fig. 2. From Fig. 4 of CH1, it can be seen that mesoscale (or anvil) rain occurred on 8 out of the 11 Phase III days sampled. The areas covered by anvil rain on each of these days are listed in Table 1. From these data, the ratio τ_m/τ for Phase III of GATE may be estimated as $^8/_{11}$ or 0.73, while the fractional area covered by mesoscale rain in Phase III, A_m/A, is estimated as 0.076. With these values, the factor $(A\tau/A_m\tau_m)$ in (51) is estimated to be $[(0.73)(0.076)]^{-1} \approx 18$.

Using this value and substituting for $M_m(p)$ from (32) for the mesoscale updraft $[p < p(z_m)]$ and from (37) for the mesoscale downdraft $[p \geq p(z_m)]$, we may write (51) as

$$w_m(p) = \begin{cases} w_{mu}(p) = 18\rho_m^{-1}(p) \\ \quad \times \left(\dfrac{C_{mu}}{A\tau}\right)f_{mu}(p)I_3^{-1}, \quad p < p(z_m) \\ w_{md}(p) = 18\rho_m^{-1}(p) \\ \quad \times \left(\dfrac{E_{md}}{A\tau}\right)f_{md}(p)I_4^{-1}, \quad p \geq p(z_m). \end{cases} \tag{52}$$

Values of the mesoscale updraft velocity $w_{mu}(p)$ computed from this relation for the 10 km (p = 285 mb) level and of the mesoscale downdraft velocity $w_{md}(p)$ computed for the 1.6 km (p = 830 mb) level are listed in Tables 2 and 3 for ranges of values of the quantities C_{mu} and E_{md}. The density $\rho_m(p)$ used in these calculations was 0.42 kg m^{-3} for the 285 mb level and 1 kg m^{-3} for the 830 mb level.

From (40) and (41), it is recalled that C_{mu} and E_{md} are functions of the water budget parameters. As will be explained in later sections, the values of C_{mu} and E_{md} given in Tables 2 and 3 are those allowed by the various combinations of water budget parameters that satisfy the constraints (42) and (47) discussed above. None of the magnitudes of w_{mu} and w_{md} given in Tables 2 and 3 seem unreasonably large for mesoscale updrafts or downdrafts. Evidence from both observations and models indicates that well-defined mesoscale downdrafts are ~10 cm s^{-1} in absolute value (Zipser, 1977; Zipser and Gautier, 1978; Brown, 1979; Leary and Houze, 1980; Leary, 1980). Less evidence is available for the mesoscale updrafts, but Brown's (1979) model shows mesoscale updrafts of similar order though somewhat larger (in absolute value) than the mesoscale downdrafts.

The values of w_{mu} and w_{md} in Tables 2 and 3 are averages for an ensemble of clouds which probably contains both weak and strong anvil cloud circulations. These averages, therefore, could be substantially less than values found in individual case studies. Nevertheless, we consider the absence of significant mesoscale motions in the ensemble averages to be highly unlikely and require any reasonable set of water budget parameter to produce results for which the mesoscale vertical velocities are within an order of magnitude of the upper ends of the ranges given in Tables 2 and 3. Since the largest updraft magnitude is ~30 cm s^{-1} and the largest downdraft magnitude is ~10 cm s^{-1}, these constraints may be stated as

$$w_{mu}\ (285\ \text{mb}) > 3\ \text{cm s}^{-1}, \tag{53}$$

$$w_{md}\ (830\ \text{mb}) < -1\ \text{cm s}^{-1}. \tag{54}$$

6. Assumptions to simplify the forms of the water budget parameters

Before using the five constraints, (42), (47), (48), (49), (53) and (54), discussed in the preceding section, to identify the physically reasonable values of the water budget parameters ν_c, ν_m, α, a, η, β and b, we make some assumptions to simplify the mathematical forms of the parameters.

First, we let

$$\nu_c(\lambda) = \text{constant for all } \lambda. \tag{55}$$

Although this assumption is primarily for mathematical convenience, it may be justified since we are considering only the deeper, precipitating clouds of the tropics. If the whole spectrum of clouds was being considered, a functional form with ν_c increasing from zero for shallow cumulus to some positive value for deep cumulonimbus would have to be used.

TABLE 1. Area covered by mesoscale (i.e., anvil) rain at 1200 GMT within the 1.87 × 10^5 km^2 region covered by the *Oceanographer* radar on the 11 days of Phase III of GATE studied by Cheng and Houze (1979).

Day	Area covered by mesoscale rain within the radar area (km^2)	Fraction of the radar area covered by mesoscale rain
30 Aug 1974	0	0
31 Aug 1974	1.86 × 10^3	0.01
1 Sep 1974	1.72 × 10^3	0.01
2 Sep 1974	2.28 × 10^4	0.12
3 Sep 1974	0	0
4 Sep 1974	1.73 × 10^4	0.09
5 Sep 1974	3.50 × 10^4	0.19
6 Sep 1974	1.65 × 10^4	0.09
7 Sep 1974	0	0
9 Sep 1974	1.41 × 10^4	0.06
10 Sep 1974	7.1 × 10^3	0.04
Average for eight days with nonzero values	1.42 × 10^4	0.076

TABLE 2. Vertical velocities at the 10 km (p = 285 mb) level in the mesoscale updraft (w_{mu}) for a range of values of mesoscale updraft condensation C_{mu}. Values of the condensation are expressed per unit area and time by dividing C_{mu} by the constant factors A and τ.

$C_{mu}/A\tau$ (kg m^{-2} h^{-1})	w_{mu} (cm s^{-1})
0.01	3
0.02	6
0.05	14
0.075	21
0.10	28
0.12	34

In CH1, we found that anvil precipitation was associated almost exclusively with deep convection (echo tops ≥7 km). We assume, here, therefore, that anvil clouds incorporate condensate only from cells with tops extending above height z_A = 7 km (430 mb). For these cells, then, $\eta(\lambda)$ has a finite value, while for shallower cells $\eta(\lambda) = 0$. Accordingly, we let

$$\eta(\lambda) = \begin{cases} \eta_A = \text{constant} > 0, & \text{for} \quad \lambda < \lambda(z_A) \\ 0, & \text{for} \quad \lambda > \lambda(z_A). \end{cases} \tag{56}$$

As in LH, we assume, in the absence of other information, that reevaporation of condensate in the large-scale environment (represented by water budget parameters β and b) is a minor factor in the water budgets of both deep convective cells and anvil clouds. For mathematical convenience, β and b are expressed as fractions of the downdraft evaporation parameters $\alpha(\lambda)$ and a, respectively,

$$\beta(\lambda) = \phi_c\alpha(\lambda), \quad \text{for} \quad \lambda \leqslant \lambda(z_A), \tag{57}$$

$$b = \phi_m a, \tag{58}$$

where $\phi_c = 0.54$ and $\phi_m = 0.25$ (the values used by LH). For the values of α and a considered below, these values of ϕ_c and ϕ_m ensure that $\beta \leqslant 0.14$ [for $\lambda \leqslant \lambda(z_A)$] and $b \leqslant 0.12$.

TABLE 3. Vertical velocities at the 1.6 km (830 mb) level in the mesoscale downdraft for a range of values of mesoscale downdraft evaporation E_{md}. Values of the evaporation are expressed per unit area and time by dividing E_{md} by the constant factors A and τ.

$E_{md}/A\tau$ (kg m^{-2} h^{-1})	w_d (cm s^{-1})
0.009	−0.8
0.020	−1.6
0.033	−2.6
0.047	−3.8
0.064	−5.2
0.085	−6.8
0.110	−8.8
0.140	−11.4

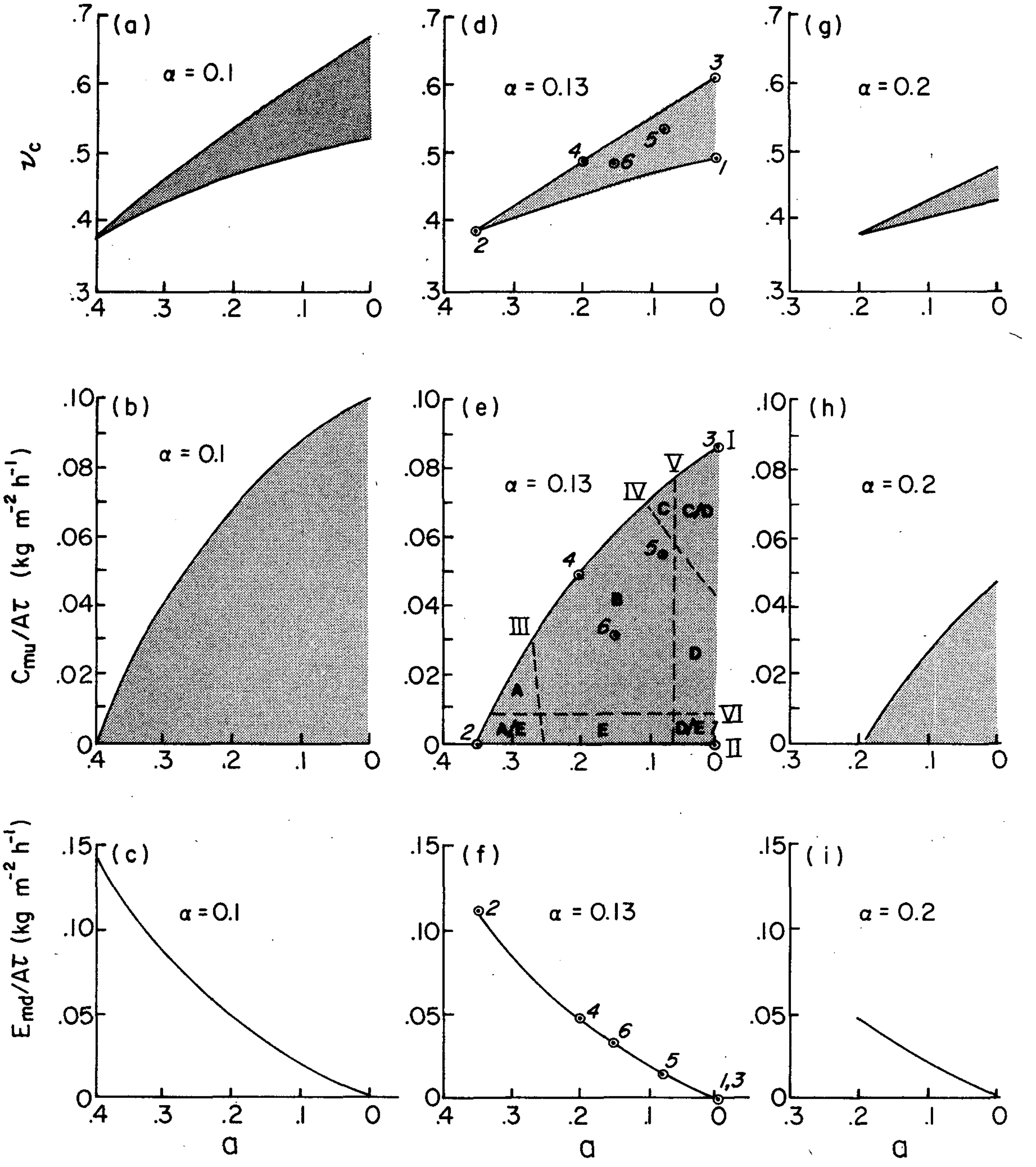

FIG. 5. Convective precipitation efficiency ν_c, mesoscale updraft condensation rate $C_{mu}/A\tau$, and mesoscale downdraft evaporation rate $E_{md}/A\tau$ as functions of the water budget parameters α and a. Shading covers domains of ν_c and $C_{mu}/A\tau$ satisfying the constraints (42) and (47). Region B is the domain of most reasonable results. Curves I-VI and regions A, C, D and E are explained in the text. Points 1-6 represent cases for which mass and heat flux profiles are computed and shown in Figs. 8 and 9.

Also for simplicity, we let the fractional reevaporation in convective downdrafts $\alpha(\lambda)$ be the same for all cloud sizes, i.e.,

$$\alpha(\lambda) = \text{constant for all } \lambda. \qquad (59)$$

This assumption, with (6), (55), (56) and (57) implies, since $\eta(\lambda)$ decreases from η_A to 0 from deep [$\lambda \leq \lambda(z_A)$] to shallow [$\lambda > \lambda(z_A)$] clouds, that the fractional reevaporation of condensate in the environment $\beta(\lambda)$ is greater for shallow than deep clouds. Such a property seems qualitatively realistic. This property of $\beta(\lambda)$ is purely implicit since in our study $\beta(\lambda)$ does not enter any calculations.

7. Amount of mesoscale updraft and downdraft motion allowed by the physically reasonable combinations of water budget parameters

Making use of the simplifying assumptions (55)–(59), we may now use the criteria (42), (47), (48), (49), (53) and (54) to identify the physically reasonable values of the water budget parameters and, from these values, determine the magnitudes of mesoscale updraft and downdraft mass and heat fluxes allowed by the physically reasonable combinations of parameters. Since the fluxes of mass and heat by the mesoscale updrafts are proportional to the amount of condensation C_{mu} produced by the upward motion [(32) and (33)] and the mesoscale downdraft mass and heat fluxes are proportional to the amount of evaporation E_{md} associated with the downward motion [(37) and (38)], we proceed by determining the values of C_{mu} and E_{md} for various combinations of water budget parameters.

a. Expression for C_{mu} and E_{md} as functions of water budget parameters

To express C_{mu} in terms of water budget parameters, (55), (56) and (59) may be substituted into (40) to obtain

$$C_{mu} = \frac{R_m}{\nu_m} - \frac{\eta_A}{\nu_c}\int_0^{\lambda(z_A)} R_c d\lambda. \tag{60}$$

The integral in the last term is the total rain from deep convective cells (those with tops above $z_A = 7$ km) and may be written

$$\mathcal{R}_{CA} = \int_0^{\lambda(z_A)} R_c d\lambda = \text{constant}. \tag{61}$$

With the aid of (6), (56) and (57), η_A may be written as

$$\eta_A = 1 - (1 + \phi_c)\alpha - \nu_c. \tag{62}$$

Substituting (58) into (12) and rearranging terms leads to

$$\nu_m = 1 - (1 + \phi_m)a. \tag{63}$$

Substituting (61)–(63) in (60), we obtain

$$C_{mu} = \frac{1}{1 - (1 + \phi_m)a} R_m - \frac{1 - (1 + \phi_c)\alpha - \nu_c}{\nu_c}\mathcal{R}_{CA}. \tag{64}$$

In this form, C_{mu} can be seen to depend only on the three water budget parameters α, ν_c and a, since the mesoscale anvil precipitation R_m and the total precipitation from deep convective cells $\mathcal{R}_{CA}$ are observed quantities and the quantities ϕ_c and ϕ_m are assumed constant.

To express E_{md} in terms of water budget parameters, (63) may be substituted in (41) to obtain

$$E_{md} = \frac{a}{1 - (1 + \phi_m)a} R_m. \tag{65}$$

In this form, E_{md} can be seen to depend only on the water budget parameter a since R_m is observed and ϕ_m is assumed constant.

From (64) and (65), it is evident that the amounts of mesoscale updraft and downdraft motion in the cloud ensemble, indicated by C_{mu} and E_{md}, respectively, depend entirely on ensemble rainfall amounts and the three water-budget parameters, α, ν_c and a. The physical roles of these three free parameters may be seen by noting that as the mesoscale downdraft evaporation parameter a increases, not only does the mesoscale downdraft motion increase according to (65), but the first term on the right-hand side of (64) also increases; i.e., more condensate must be provided to the anvil in order to provide the required R_m. However, if the convective updraft precipitation efficiency ν_c and the convective downdraft evaporation parameter α are both sufficiently small when a is large, the second term on the right of (64) counteracts the first term, and C_{mu} is small or zero. Physically, this cancellation occurs because the low efficiency of the cells implies, according to (62), a large η_A. That is, the excess condensate not rained out in the cells is transferred to the anvil and production of condensate by a mesoscale updraft in the anvil itself is not required. If, however, ν_c is large when a is large, the second term on the right of (64) is small, the first term on the right of (64) is not offset by the second term, and C_{mu} is large. Physically, this occurs because the high efficiency of the cells implies, according to (62), that α and η_A are small. The small η_A means that little excess condensate is available to be transferred to anvils from cells and production of condensate by a mesoscale updraft in the anvil itself is therefore required.

b. Identification of physically reasonable results

It follows from (64) and (65), that by finding the physically reasonable values of α, ν_c and a allowed by the constraints (42), (47)–(49), (53) and (54) and substituting these values in (64) and (65), we may identify the physically reasonable values of C_{mu} and E_{md}.

We proceed by applying at first only the constraints (42) and (47). The values of ν_c and a allowed by these two constraints are shown by the shaded areas in Figs. 5a, 5d and 5g, for values of $\alpha = 0.1$, 0.13 and 0.2. The corresponding values of C_{mu}, computed from (64), are shown by the shaded areas in Figs. 5b, 5e and 5h. The allowable values of E_{md}, computed from (65), are shown in Figs. 5c, 5f and 5i. The values of E_{md} are shown by a curve rather than an area since E_{md} depends only on a.

The upper boundary of each shaded area in Fig. 5 is determined from the equality in constraint (47). This boundary is referred to as curve I in Fig. 5e. The lower boundary of each shaded area (curve II in Fig. 5e) is determined by the equality in constraint (42). As required by (42), this boundary lies along the abscissae of Figs. 5b, 5e and 5h.

c. Mutual exclusiveness of strong anvil updrafts and strong anvil downdrafts

From Fig. 5, it is seen that, as a decreases, the upper boundary of the region of possible C_{mu} (e.g., curve I in Fig. 5e) increases while E_{md} decreases sharply. That is, the anvil updrafts and mesoscale downdrafts below the anvils cannot simultaneously have their maximum effects without violating the constraint (47).[3] This result is consistent with the results of LH, who showed that, for a given amount of precipitation, the inclusion of either mesoscale updrafts or downdrafts or both leads to the diagnosis of larger heat transports in the middle to upper troposphere [where constraint (47) is applied] than if the precipitation is explained by purely convective drafts (curves B and C, Fig. 9 of LH).

d. Inability of strong convective-scale downdrafts to coexist with strong mesoscale motions.

Figs. 5b, 5e and 5h show that as α is increased from 0.1 to 0.2, the domain of physically reasonable results (size of shaded area) shrinks. By definition, the value $\alpha = 0.1$ means that only 10% of the convective condensate was reevaporated in convective-scale downdrafts. Since it seems unlikely that convective-scale downdrafts would have less than this much effect, $\alpha = 0.1$ must be near the lower limit of α. The upper limit of α is harder to establish. However, from Fig. 5, it is evident that, as α increases, the maximum values of C_{mu} and E_{md} allowed by the constraints (42) and (47) both decrease sharply. That is, strong convective-scale downdrafts ($\alpha \geqslant 0.2$) cannot co-exist with substantial mesoscale updraft and downdraft motion.

The reason for this result can be seen by considering the combination of C_{mu} and a corresponding to any one point on curve I of Fig. 5e. Since the equality in (47) is satisfied everywhere along this curve, $\mathcal{H}$ (285 mb) = $\mathcal{H}^*$ (285 mb) for the considered combination of C_{mu} and a, when $\alpha = 0.13$. If α is increased, this same combination of C_{mu} and a must be associated with a lower value of the convective precipitation efficiency ν_c. This result can be seen by holding C_{mu} and a constant and increasing α in (64). Since, according to (28), the decreased efficiency implies greater heat transport by convection, for the given amount of convective rain and since C_{mu} (and hence $\mathcal{H}_{mu}$) is unchanged, $\mathcal{H}$ (285 mb) is increased, and (47) is now violated. Therefore, any point in the C_{mu}-a plane that lies on curve *I* when $\alpha = 0.13$ lies outside the domain of acceptable combinations of C_{mu} and a when α is increased. Thus, the domain of acceptable values of C_{mu} and a is seen to shrink, and the maximum values of C_{mu} (obtained when $a = 0$) is seen to decrease when α is increased (cf. Figs. 5b, 5e and 5h). Since the maximum value of a (at the left-hand end of the shaded area in Figs. 5b, 5e and 5h) decreases as the domain shrinks, the maximum value of E_{md} (obtained at the left-hand end of the curves in Figs. 5c, 5f and 5i) also decreases as α is increased. Thus, the maximum possible values of both C_{mu} and E_{md} decrease with increasing α.

Since, by this reasoning, large mesoscale motions cannot co-exist with strong convective-scale downdrafts, we need only to consider results for $\alpha \approx 0.1$–0.2 to determine the effects of mesoscale vertical motion on ensemble vertical transports. We will focus on $\alpha = 0.13$ (Figs. 5d–5f), since this was the value used by LH.

e. Existence of weak and strong mesoscale downdrafts in the cloud ensemble

Another result indicated by Fig. 5 is that the domain of possible results always lies between $a = 0$ and 0.4 (the latter value marks the left-most extent of the curves in Figs. 5a–5c). In LH, a value of $a = 0.4$ was found to apply to an intense tropical anvil cloud system. Most of the results allowed by our constraint (shaded areas in Fig. 5), however, lie well to the right of $a = 0.4$ (i.e., toward lower values of a) in Fig. 5. This apparent paradox is explained by the fact that the result of LH applies to the downdraft of a well-defined, strong anvil cloud system of the type examined in case studies (e.g., Zipser, 1969, 1977; Houze, 1977; Leary and Houze, 1979), whereas our values of a apply to an ensemble of clouds which probably contains a spectrum of weak to strong anvil cloud systems.

This explanation may be more clearly seen from the mathematical form of a, which can be obtained by substituting (34) and (65) in the left and right sides, respectively, of (37) to obtain

$$\mu_{md} = \frac{aR_m}{(1 - 1.25a)I_4} . \qquad (66)$$

Solving this expression for a, we obtain

$$a = \frac{r}{1 + 1.25r} , \qquad (67)$$

where

$$r = \left(\frac{\mu_{md}}{R_m}\right)I_4. \qquad (68)$$

The function $a(r)$ is plotted in Fig. 6 for $a = 0$ to 0.4.

---

[3] This statement is strictly true only if the moist static energy difference in the expression (33) for $\mathcal{H}_m$ is larger than some small positive value. For reasonable values of the moist static energy difference the statement is valid. The sensitivity of our results to the moist static energy difference are considered in Section 7g.

In LH, μ_{md} was determined by using Leary's (1980) model to find the rate at which air is transported downward (per unit area and time) in a strong anvil downdraft that produces a large modification of temperature and humidity profiles below the anvil. To determine μ_{md}, this rate was applied by LH to an anvil of typical horizontal extent and duration. Now, substituting this value of μ_{md} along with the total rain R_m of the intense anvil in (68) gives a value of r, which in turn, leads to a value of $a = 0.4$, when substituted in (67).

Since the μ_{md} and R_m in our study are totals for an ensemble, which likely contains both weak[4] and strong anvils, our values of r and a should be lower than those of LH, which apply to the strong anvil downdraft cases. It is reasonable, therefore, that our constraint on the heat flux profile [Eq. (47), which produces the upper bounds (e.g., curve I) of the shaded areas in Fig. 5], together with the constraint on C_{mu} [Eq. (42), which produces the lower bounds (e.g., curve II) of the shaded areas in Fig. 5], indeed gives the preponderance of possible results at values of a considerably <0.4. That is, the cloud ensemble must be assumed to contain at least some weak anvils or it will not be likely to produce a realistic heat flux profile.

f. Narrowing the range of possible results by the application of further constraints

The domains of physically reasonable results shown by the shaded areas in Fig. 5 [which are determined by the constraints (42) and (47)] can be reduced by applying the constraints (48), (49), (53) and (54). To illustrate this, we will concentrate on the results for $\alpha = 0.13$, shown in Figs. 5d–5f. In particular, we will analyze the shaded area in Fig. 5e, where Region A, bounded by curve III, is eliminated by constraint (48). These solutions have too large a heat flux at the top of the subcloud layer (e.g., curve 2 in Fig. 8b, which is discussed in Section 8a; see especially footnote 5). Region C, bounded by curve IV, is eliminated by constraint (49). These solutions have too high a precipitation efficiency. Region D, bounded by curve V, is eliminated by constraint (54). These solutions have too little mesoscale downdraft motion. Region E is eliminated by constraint (53). These solutions have too little mesoscale updraft motion. Overlaps of the eliminated regions are denoted C/D, D/E and A/E. The domain of acceptable results is reduced to Region B, which lies in the center of the shaded region and is not eliminated by any of our constraints.

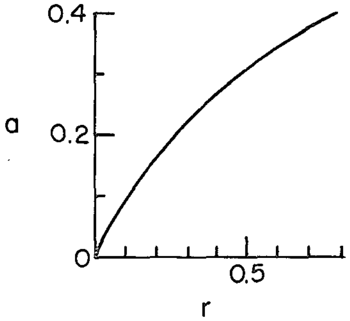

FIG. 6. Mesoscale downdraft evaporation parameter a as a function of the quantity r, which is defined by (68) and is proportional to the ratio of the mass of air transported in the mesoscale downdraft below anvil clouds to the amount of mesoscale rainfall reaching the surface from the anvil.

g. Sensitivity of results to assumed mesoscale updraft structure

The size of region B, which contains the results deemed physically reasonable by our constraints, is determined primarily by constraint (47), which locates the upper boundary of the region (curve I). The upper boundary of region B is given by the maximum value of mesoscale updraft condensation C_{mu} allowed by this constraint. From (33), it is evident, however, that the contribution of $\mathscr{H}_m(p)$ to $\mathscr{H}(p)$ in (47) depends not only on C_{mu} but also on the shape of the profile of mass flux in the mesoscale updraft f_{mu} and on the moist static energy difference $(h_{mu} - \bar{h}_e)$ between the mesoscale updraft and the large-scale environment. In this section, we test the sensitivity of the size of region B to assumptions about f_{mu} and $(h_{mu} - \bar{h}_e)$. As explained in the Appendix, the shape of the profile $f_{mu}(z)$ is controlled by the height $z_{\max}$ where the profile is assumed to have its peak value, while the moist static energy difference is controlled by the assumed temperature difference ΔT between the mesoscale updraft and the large-scale environment. It is further noted in the Appendix that all calculations in this paper, except where otherwise stated, are for the values $z_{\max} = 10$ km and $\Delta T = 1$°C. Region B in Fig. 5 was determined using these values. This same region is shown by the shaded area in Fig. 7. Fig. 7 shows the changes in region B obtained when alternate combinations of $z_{\max}$ and ΔT are used. Curve 1 shows that as $z_{\max}$ is decreased from 10 to 7 km (i.e., the peak mass flux occurs lower in the anvil cloud) the upper boundary is raised and the size of region B is increased. Curve 2 shows that the upper boundary of region B is also raised when ΔT is lowered from 1.0 to 0.5°C. As ΔT is decreased, $(h_{mu} - \bar{h}_e)$ is reduced, and larger values of C_{mu} can be allowed according to (33), without violating the constraint (47). Conversely, when ΔT is increased from 1.0 to 1.5°C, the maximum C_{mu}

---

[4] By "weak" anvil, we mean one for which a [$=E_{md}/(C_{mu} + C_A^*)$ according to (10)] is small. That is, only a small fraction of the total anvil condensate $(C_{mu} + C_A^*)$ is evaporated in a mesoscale downdraft. The mesoscale downdraft is weak or does not develop well enough to evaporate much of the precipitation falling from the anvil.

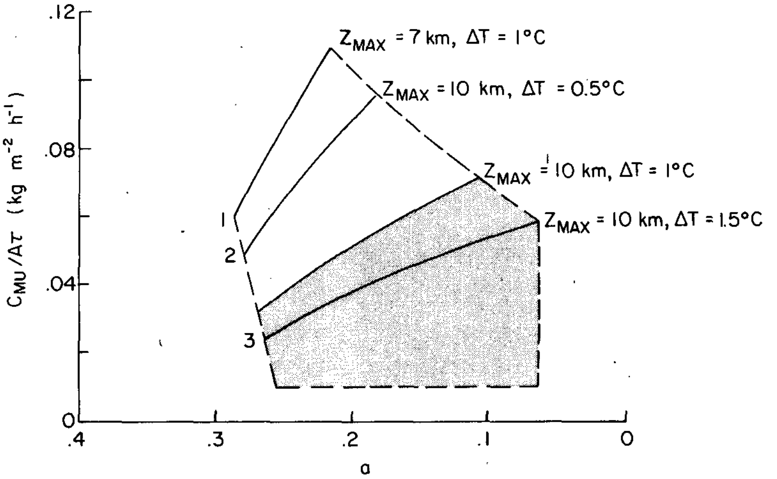

FIG. 7. Sensitivity of the domain of physically reasonable results to assumptions about mesoscale updraft structure. Region B, the domain of most reasonable results shown in Fig. 5, is shaded. Curves 1, 2 and 3 show the boundary of region B obtained under different assumptions about mesoscale updraft structure. $z_{\max}$ is the height at which the mesoscale updraft mass flux profile is assumed to have its peak value. ΔT is the assumed temperature difference between the mesoscale updraft and its large-scale environment.

allowed by (47) is reduced and the size of region B is decreased (curve 3).

We conclude that our choices of $z_{\max} = 10$ km and $\Delta T = 1°\mathrm{C}$ are rather conservative. Most other choices, according to Fig. 7, would lead to an increase in the size of region B with larger possible values of C_{mu}. Our conclusions in subsequent sections regarding the possible effects of mesoscale anvil air motions would be even more pronounced if $z_{\max}$ or ΔT are actually lower than 10 km or 1°C, respectively. Only if ΔT is $>1°\mathrm{C}$, would the conclusions of this paper tend toward an overstatement of the possible role of mesoscale motions.

8. Mass and heat flux profiles for various combinations of mesoscale updraft and downdraft motions

In this section, we examine the profiles of mass and heat flux computed for the various combinations of water budget parameters allowed by our constraints. We consider six representative combinations of parameters, which are listed in Table 4, indicated by points 1–6 in Figs. 5d–5f, and hereafter referred to as cases 1–6. In case 1 (lower right of Figs. 5d–5f), there are no mesoscale motions ($C_{mu} = E_{md} = 0$). The heat flux for case 1 was referred to as $\mathscr{H}^*(p)$ in Section 5c. Case 1 will be used in this section as the reference to which other cases are compared. Since all the other cases involve mesoscale motions to some degree, comparison with case 1 indicates how much the results in each case are affected by including mesoscale motions.

We consider first cases 2 and 3. Case 2 has the maximum amount of mesoscale downdraft motion allowed by the two constraints (42) and (47); i.e., E_{md} is maximum for case 2 (Fig. 5f). Case 3, on the other hand, has the maximum mesoscale updraft motion allowed by these constraints (maximum C_{mu} in Fig. 5e). The mutually exclusive property of strong mesoscale updrafts and downdrafts noted in Section 7c, requires, however, that case 2 (the maximum mesoscale downdraft case) has no mesoscale updraft at all and that case 3 (the maximum mesoscale updraft case) has no mesoscale downdraft. Therefore, these extreme cases will serve to illustrate qualitatively the isolated effects of mesoscale downdrafts and updrafts. However, both cases 2 and 3 lie well outside the region B, which contains the physically most reasonable cases obtained when the full set of constraints [(42), (47)–(49), (53) and (54)] is applied. Cases 4–6, which contain moderate amounts of both mesoscale updraft and downdraft motion, lie within region B and serve to represent the most plausible cases. In the following subsections, we consider, in turn, the extreme cases 2 and 3 and then the physically reasonable cases 4–6.

TABLE 4. Values of water budget parameters for various cases.

Case	α	a	ν_c
1	0.13	0	0.50
2	0.13	0.35	0.38
3	0.13	0	0.61
4	0.13	0.20	0.49
5	0.13	0.08	0.54
6	0.13	0.15	0.49

a. Extreme cases

Cases 2 and 3 are compared with case 1 in Fig. 8. In both cases 2 and 3, the mass flux is greater in the upper troposphere and less in the lower troposphere than in case 1 (Fig. 8a). However, the reasons for the redistribution of the mass transport in the vertical are quite different in the two cases.

In case 2, the redistribution of mass flux arises because of the increase in the water budget parameter a, which determines the amount of evaporation in the mesoscale downdraft. A larger a requires that more water must fall from the base of the anvils to supply the increased mass of water evaporated in the mesoscale downdrafts below the anvils. An increase in convective-scale updraft motion is therefore required to condense this extra water and supply it to the anvils [through the term C_A^* in (7)] since there are no mesoscale updrafts in the anvil clouds themselves in this case. At low levels, this increase in convective-scale updraft motion is more than offset by the mesoscale downdraft motion. Thus, there is a net reduction in the ensemble mass flux in the lower half of the troposphere (below 600 mb). Aloft, above the level of the tops of the mesoscale downdrafts, the convective updraft mass flux is not offset in this way and the net ensemble mass flux is increased.

In case 3 the vertical redistribution of the computed mass flux is explained not by the presence of mesoscale downdrafts below anvil clouds (since they do not exist in this case), but rather by the presence of mesoscale updraft motions within the anvils themselves. The mesoscale updraft motion, which all occurs above the bases of the anvils, explains the increased mass transport in upper levels. The reduced mass transport at low levels is the result of the reduced amount of convective updraft motion required in cells when the condensate in anvils is explained by mesoscale updrafts aloft [term C_{mu} in (7)] rather than by the convective-scale updrafts in neighboring cells.

Whereas the mass flux profiles in Fig. 8a show similar responses to the inclusion of mesoscale downdraft (case 2) and updraft (case 3) motions, the heat flux profiles in Fig. 8b show opposite responses. In case 2, the heat flux in the lower troposphere is increased compared with case 1,[5] while in case 3 it is reduced.

The increase of heat flux in the lower troposphere in case 2 is related to the combined effects of (i) the large mesoscale downdraft motion, which is present in the lower troposphere in this case, and (ii) the increased convective-scale updraft motion in cells, which is required to supply condensate to the anvil, since there is no mesoscale updraft motion in this case. These two effects reinforce since both the convective-scale updrafts and the mesoscale downdraft motion contribute to upward heat flux.

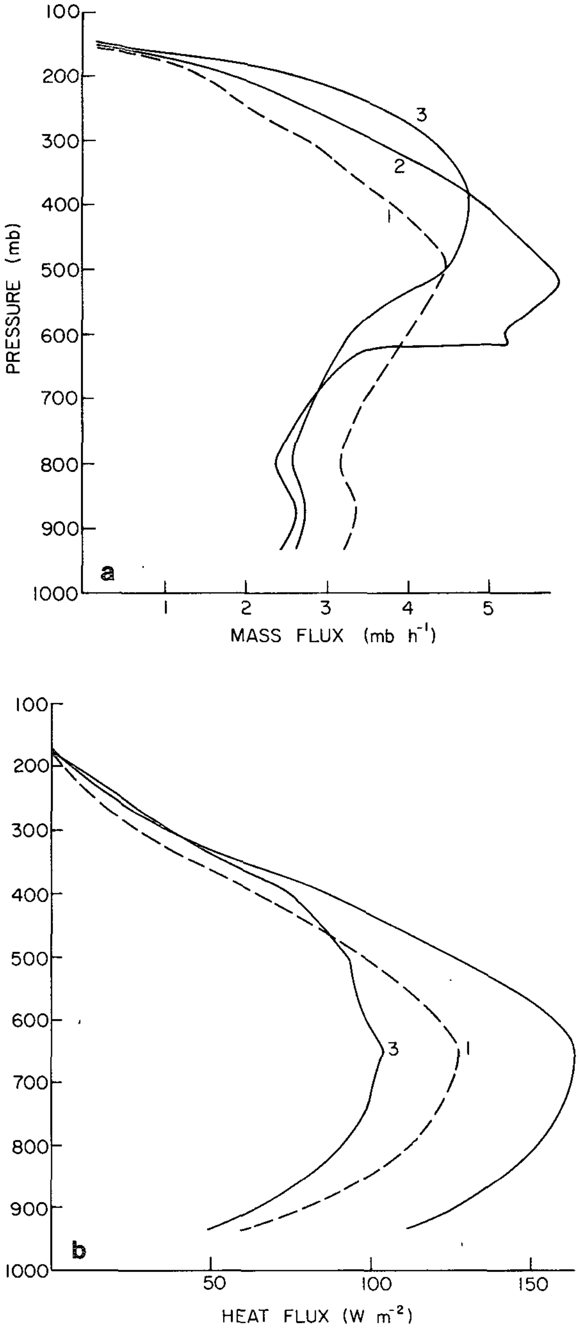

FIG. 8. Cloud ensemble mass (a) and heat fluxes (b) for extreme assumptions about mesoscale updrafts and downdrafts. Numbers refer to cases discussed in text. Case 2 is for maximum mesoscale downdraft motion and no mesoscale updrafts. Case 3 is for maximum mesoscale updraft motion and no mesoscale downdrafts. Case 1, shown for comparison, is for no mesoscale updrafts or downdrafts. Mass flux, given by $M(p)$ in text, has been multiplied by the gravitational acceleration to obtain units of mb h^{-1}.

---

[5] The increase is so great that constraint (48) is violated. Note that case 2 lies to the left of curve III in Fig. 5e.

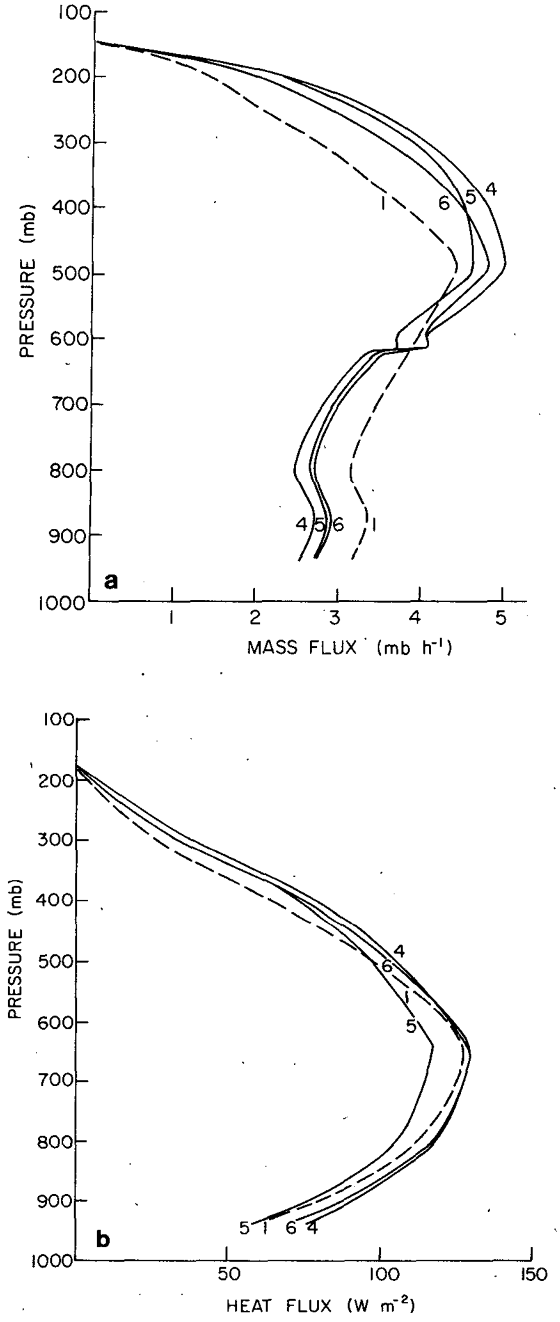

FIG. 9. Cloud ensemble mass and heat flux for reasonable assumptions about mesoscale updrafts and downdrafts. Numbers refer to cases discussed in text. Cases 4, 5 and 6 all contain moderate amounts of both mesoscale updraft and downdraft motion. Case 1, shown for comparison, is for no mesoscale updrafts or downdrafts. Mass flux, given by $M(p)$ in text, has been multiplied by the gravitational acceleration to obtain units of mb h^{-1}.

The decrease of heat flux in the lower troposphere in case 3 is explained by the reduced amount of convective-scale updraft motion required in cells when the condensation in anvils is explained by the existence of mesoscale updrafts aloft within the anvils themselves. At upper levels, the decreased heat flux by convective-scale drafts is offset by the increased heat flux by the mesoscale updraft motion. However, in the lower troposphere, below the bases of the anvils, there is a net decrease of heat flux, since there are no mesoscale downdrafts or updrafts at these levels to offset the decreased convective-scale flux.

The results of cases 2 and 3 illustrated in Fig. 8, are qualitatively consistent with results obtained in LH when mesoscale updrafts and downdrafts were included in computations of the mass and heat fluxes by a single cloud system.

b. Physically reasonable cases

The extreme cases, just examined, illustrate that either mesoscale updrafts or downdrafts acting alone lead to more upward mass flux in the upper troposphere and less mass flux in the lower troposphere than would be computed under the assumption of no mesoscale motions. It is not surprising, then, that the physically reasonable cases 4–6, which contain moderate amounts of both mesoscale updraft and downdraft motion, all show greater mass flux aloft (above ≈ 600 mb) and less mass flux at lower levels than case 1 (Fig. 9a). The reduction in mass flux at 800 mb ranges from 15% in case 6 to 22% in case 4. The increase in mass flux at 350 mb is from 19% in case 6 to 30% in case 4.

It was also shown in the previous subsection that while the effects of mesoscale updrafts and downdrafts on the mass flux profile are similar, leading to increases in mass flux aloft and decreases at lower levels, their effects on the heat flux oppose each other. The inclusion of mesoscale updrafts leads to decreased heat flux at low levels, whereas the inclusion of mesoscale downdrafts leads to increased heat flux at low levels. Since, in cases 4–6, moderate amounts of both mesoscale updrafts and downdrafts are included, these opposing effects on the heat flux tend to cancel. Consequently, the heat flux profiles for the physically reasonable cases (Fig. 9b) differ very little from the heat flux profiles for case 1, which ignores mesoscale updrafts and downdrafts.

9. Conclusions

The inclusion of mesoscale anvil updrafts and downdrafts in the diagnosis of cloud ensemble vertical transports is controlled through assumptions about the water budgets of the model cloud used to represent the actual ensemble. We have considered the entire range of water budget assumptions and rejected or deemphasized all but the physically most realistic assumptions. We require that the diagnosed heat flux at upper levels not deviate significantly from the cloud ensemble heat flux shown by synoptically derived large-scale heat budgets. Furthermore, we consider as unlikely any ensembles of clouds which do not have a substantial number of small nonprecipitating cumulus, which have convective cells which are unrealistically efficient at converting condensate to precipitation or which have too little mesoscale updraft and downdraft motion. These constraints considerably limit the choices of acceptable water budget assumptions.

Within the acceptable range, the effects of various combinations of assumed mesoscale updrafts and downdrafts on the diagnosis of ensemble mass and heat fluxes are determined by comparing the computed fluxes to those calculated under the usual assumption of no mesoscale motion. The mesoscale updrafts and downdrafts are found to act in the same sense and therefore reinforce each other in vertically redistributing the diagnosed mass flux. The inclusion of reasonable combinations of mesoscale updrafts and downdrafts leads to the diagnosis of some 15–20% less ensemble mass transport at low levels and 20–30% greater mass flux aloft than in the case of no mesoscale motion. In contributing to diagnosed ensemble heat fluxes, the mesoscale updrafts and downdrafts oppose each other. In the lower half of the troposphere, heat flux is increased when mesoscale updrafts are incorporated and decreased when mesoscale updrafts are included. All the realistic choices of assumptions involve a combination of mesoscale updraft and downdraft motion. The opposing effects of these drafts on the heat flux tend to cancel and the profile of heat flux, consequently, is not much different than in the typically assumed but physically unrealistic case of no mesoscale vertical motions.

From these results, it appears that schemes for diagnosing or parameterizing the effects of tropical cloud populations may not be in much error in ignoring the effects of anvil updrafts and downdrafts on ensemble heat fluxes. However, the vertical distribution of mass flux by the deep precipitating clouds might be substantially in error, with too much mass flux at low levels and too little aloft. This significant difference in the vertical distribution of mass flux indicates further that there is the potential for error in other computed cloud-ensemble quantities, such as the vertical distribution of latent heat release, which is directly proportional to the mass flux profiles, or momentum and vorticity fluxes. Future studies should be directed toward evaluating the effects of mesoscale anvil air motions on these quantities.

APPENDIX

Mass Flux Profiles, Entrainment Rates and Thermodynamic Properties of Model Cloud Updrafts and Downdrafts

The mass flux profiles, f_u, f_d, f_{mu} and f_{md}, the entrainment rate versus cell height relationship λ_T, and the updraft and downdraft moist static energies, h_u, h_d, h_{mu} and h_{md}, which we use in computing the mass and heat fluxes by an ensemble of clouds, are given by relationships presented in H and further discussed in CH2 and LH. Here we describe the assumptions that we make in order to specialize the relationships of H for use in the present study.

1. Assumptions about convective-scale updrafts and downdrafts

As explained in H, the properties of convective-scale drafts are computed using one-dimensional steady-state plume models in which f_u and f_d have prescribed shapes, $\lambda_T(p)$ is the inverse of $p_T(\lambda)$, where $p_T(\lambda)$ is the pressure at height $z_T(\lambda)$, which is the level of zero buoyancy of any updraft with entrainment rate λ, $h_u[\lambda, p(z)]$ is obtained by integrating the first law of thermodynamics upward from cloud base z_B to height $z_T(\lambda)$, and $h_d[\lambda, p(z)]$ is obtained by integrating the first law downward from the downdraft starting level z_0 to cloud base z_B. To carry out these calculations we make the following assumptions, which follow the recommendations given in the conclusions of CH2.

a. Relationship between convective cell height and entrainment rate

For this relationship, we use the smoothed curve in Fig. 4 of H.

b. Mass flux profiles

For the convective-scale updrafts, we use the truncated Austin and Houze (1973) mass flux profile expressed by Eqs. (5)–(7) of CH2. According to this profile, most detrainment occurs below cloud top but is concentrated in the upper one-fourth of the cell height. The convective-scale downdrafts are assumed to have the inverted convective updraft mass flux profile expressed by Eqs. (8) and (9) of CH2. The convective downdraft starting level z_0 is specified in the same way as in Johnson (1976).

c. Thermodynamic properties of entrained air

The moist static energy and water vapor mixing ratio of the air entrained into the convective-scale drafts are assumed to be those of the large-scale environment.

d. Boundary conditions for the convective updrafts and downdrafts

The cloud base condition of Johnson (1976) is used, in which the virtual temperature excess at the base z_B of the updrafts is zero. This condition is given by Eq. (15) of Johnson (1976).

At the convective downdraft originating level z_0, the air feeding the downdraft is assumed to be saturated, with moist static energy equal to that of the environment.

2. Assumptions about mesoscale updrafts and downdrafts

Assumptions about the mesoscale drafts in our model clouds are similar to those used in LH.

a. Mass flux profiles

The mesoscale updrafts are assumed to have a parabolic mass flux profile with a normalized magnitude of 1.0 at $z = z_{\max}$. In this study we used two profiles, one with $z_{\max} = 10$ km and one with $z_{\max} = 7$ km. These profiles are given by

$$f_{mu}(z) = \begin{cases} A_1 z^2 + A_2 z + A_3, & z_m < z < z_{\max} \\ B_1 z^2 + B_2 z + B_3, & z_{\max} < z < z_{Tm}, \end{cases} \quad \text{(A1)}$$

where $z_m = 4.5$ km, $z_{TM} = 14$ km. For $z_{\max} = 10$ km, $A_1 = -0.0331$ km^{-2}, $A_2 = 0.661$ km^{-1}, $A_3 = -2.3$, $B_1 = -0.0625$ km^{-2}, $B_2 = 1.25$ km^{-1}, and $B_3 = -5.25$; for $z_{\max} = 7$ km, $A_1 = -0.16$ km^{-2}, $A_2 = 2.24$ km^{-1}, $A_3 = -6.84$, $B_1 = -0.0204$ km^{-2}, $B_2 = 0.2857$ km^{-1} and $B_3 = 0$.

For most calculations in this study, the profile for $z_{\max} = 10$ km is used. Differences in results obtained with $z_{\max} = 7$ km are discussed.

The mesoscale downdraft mass flux is assumed to be constant between the top and base of the downdraft. This profile is given by

$$f_{md}(z) = \begin{cases} 1, & z_B \leq z \leq 4.1 \text{ km} \\ 0, & \text{otherwise}. \end{cases} \quad \text{(A2)}$$

b. Thermodynamic properties of the mesoscale drafts

The temperature and water vapor mixing ratio in the mesoscale downdraft are assumed to be those calculated by Leary (1980) and given in Table 3 of LH. As in LH, the mesoscale updraft is assumed to be saturated at an increment of temperature ΔT higher than the temperature of the large-scale environment. In this study, we consider values of $\Delta T = 0.5$, 1.0 and 1.5°C.

In most of our calculations, we follow LH and use $\Delta T = 1.0$°C. Differences in results obtained with $\Delta T = 0.5$ and 1.5°C are discussed.

Acknowledgments. Extensive comments and suggestions of Prof. Colleen A. Leary of Texas Tech University and of two JAS referees led to substantial improvement of this paper. Prof. Richard J. Reed of the University of Washington also read an early version of the manuscript and offered helpful comments. This research was supported by the Global Atmospheric Research Program, Division of Atmospheric Sciences, National Science Foundation and the GATE Project Office, National Oceanic and Atmospheric Administration under Grants ATM74-14830 A01 and ATM78-16859. This paper is contribution No. 567, Department of Atmospheric Sciences, University of Washington.

REFERENCES

Austin, P. M., and R. A. Houze, Jr., 1973: A technique for computing vertical transports by precipitating cumuli. *J. Atmos. Sci.*, **30**, 400–411.

Betts, A. K., 1973: A composite cumulonimbus budget. *J. Atmos. Sci.*, **30**, 597–610.

——, R. W. Grover and M. W. Moncrieff, 1976: Structure and motion of tropical squall-lines over Venezuela. *Quart. J. Roy. Meteor. Soc.*, **102**, 395–404.

Braham, R. R., Jr., 1952: The water and energy budgets of the thunderstorm and their relationship to thunderstorm development. *J. Meteor.*, **9**, 227–242.

Brown, J. M., 1979: Mesoscale unsaturated downdrafts driven by rainfall evaporation: A numerical study. *J. Atmos. Sci.*, **36**, 313–338.

Cheng, C.-P., and R. A. Houze, Jr., 1979: The distribution of convective and mesoscale precipitation in GATE radar echo patterns. *Mon. Wea. Rev.*, **107**, 1370–1381.

——, and ——, 1980: Sensitivity of diagnosed convective fluxes to model assumptions. *J. Atmos. Sci.*, **37**, 774–783.

Frank, N. L., 1970: Atlantic tropical systems of 1969. *Mon. Wea. Rev.*, **98**, 307–314.

Houze, R. A., Jr., 1977: Structure and dynamics of a tropical squall-line system. *Mon. Wea. Rev.*, **105**, 1540–1567.

——, and C. A. Leary, 1976: Comparison of convective mass and heat transports in tropical easterly waves computed by two methods. *J. Atmos. Sci.*, **33**, 424–429.

——, C.-P. Cheng, C. A. Leary and J. F. Gamache, 1980: Diagnosis of cloud mass and heat fluxes from radar and synoptic data. *J. Atmos. Sci.*, **37**, 754–773.

Johnson, R. H., 1976: The role of convective-scale precipitation downdrafts in cumulus and synoptic-scale interactions. *J. Atmos. Sci.*, **33**, 1890–1910.

——, 1980: Diagnosis of convective-scale and mesoscale motions during Phase III of GATE. *J. Atmos. Sci.*, **37**, 733–753.

Leary, C. A., 1980: Temperature and humidity profiles in mesoscale unsaturated downdrafts. *J. Atmos. Sci.*, **37**, 1005–1012.

——, and R. A. Houze, Jr., 1979: The structure and evolution of convection in a tropical cloud cluster. *J. Atmos. Sci.*, **36**, 437–457.

——, and ——, 1980: The contribution of mesoscale motions to the mass and heat fluxes of an intense tropical convective system. *J. Atmos. Sci.*, **37**, 784–796.

Martin, D. W., and V. E. Suomi, 1972: A satellite study of cloud clusters over the tropical North Atlantic Ocean. *Bull. Amer. Meteor. Soc.*, **53**, 135–156.

Newton, C. W., 1966: Circulations in large sheared cumulonimbus. *Tellus*, **18**, 699–713.

Thompson, R. M., S. W. Payne, E. E. Recker and R. J. Reed, 1979: Structure and properties of synoptic-scale wave disturbances in the intertropical convergence zone of the eastern Atlantic. *J. Atmos. Sci.*, **36**, 53–72.

Zipser, E. J., 1969: The role of organized unsaturated convective downdrafts in the structure and rapid decay of an equatorial disturbance. *J. Appl. Meteor.*, **8**, 799–814.

——, 1977: Mesoscale and convective-scale downdrafts as distinct components of squall-line circulation. *Mon. Wea. Rev.*, **105**, 1568–1589.

——, and C. Gautier, 1978: Mesoscale events within a GATE tropical depression. *Mon. Wea. Rev.*, **106**, 789–805.